PAPER

Tunable magnetic skyrmions in spintronic nanostructures for cellular-level magnetic neurostimulation

View the article online for updates and enhancements.

Tunable magnetic skyrmions in spintronic nanostructures for cellular-level magnetic neurostimulation

Renata Saha[1], **Kai Wu**[1,3], **Diqing Su**[2] **and Jian-Ping Wang**[1,3]

[1] Department of Electrical and Computer Engineering, University of Minnesota, Minneapolis, MN 55455, United States of America
[2] Department of Chemical Engineering and Material Science, University of Minnesota, Minneapolis, MN 55455, United States of America

E-mail: wuxx0803@umn.edu (KW) and jpwang@umn.edu (J-PW)

Abstract

Electrical probes and arrays are currently ruling the market in treating neurodegenerative, sensory and cardiovascular diseases. Despite the accomplishments, their performance is limited by high power of operation, tissue inflammation, biofouling, inefficient control of electric fields and significant incompatibility for patients who are qualified to take magnetic resonance imaging tests only. Another alternative is magnetic stimulation. In this paper, we have proposed an implantable, highly tunable skyrmion-based neurostimulator (SkyNS). The displacement of magnetic skyrmions in a metallic bilayer generates a time varying magnetic field which induces an electric field gradient large enough to trigger neuron stimulation. SkyNS operates with a current of 2.71 μA and consumes a power of 1.434 nW. The effects of Dzyaloshinskii–Moriya interaction, perpendicular magnetic anisotropy and device dimensions on stable skyrmion nucleation and smooth skyrmion dynamics in a heavy metal/ferromagnetic metal bilayer have been extensively studied by micromagnetic simulation on mumax3. This work provides a proof-of-concept to exploit the material tunability of skyrmion-based spintronic nanodevices as cellular-level, ultra-low power, implantable magnetic neurostimulators.

Keywords: skyrmion, spintronic nanodevice, mumax3, cellular-level, low power, magnetic neurostimulation

S Supplementary material for this article is available online

(Some figures may appear in colour only in the online journal)

1. Introduction

Electrical stimulation of excitable tissues has a long salutary record. For instance, deep brain stimulation (DBS) implants have been used to treat Parkinson's disease, epilepsy, dystonia, tremor and obsessive compulsive disorder (OCD) [1]. Cardiac pacemakers have been used to treat cardiac arrythmia and other disorders of the heart [2]. Even cochlear implants [3] to reestablish auditory functions in addition to limbs [4]

and retinal [5] prostheses have shown quite a promising success rate. Despite such popularity, electrical implants are limited by some major technical and biological drawbacks. Technically, these electrodes are highly magnetic resonance imaging (MRI) incompatible as the radio frequency waves interact with the conductive electrode leads and induce currents which releases heat energy strong enough to cause damage of neurological tissues [6, 7]. This nuance has often been addressed as the antenna effect in DBS implants [8]. Biologically, as these stimulating electrodes are in direct contact with the tissues, they cause neuroinflammatory and

[3] Authors to whom any correspondence should be addressed.

J. Phys. D: Appl. Phys. **52** (2019) 465002

R Saha *et al*

immune reactions resulting in glial cell scarring around the electrodes [9, 10]. Eventually this results in increased impedance alongside stimulation thresholds.

Transcranial magnetic stimulation (TMS) [11, 12] has undoubtedly played a major role in treating neurological disorders such as major depression, stroke and chronic pain. This technique involves holding a coil over the scalp which generates a time-varying magnetic field (~1 T) that induces a current for neuromodulation. Although this magnetic field is highly permeable through biological tissues, the spatial-selective control of TMS is limited due to the bulky instrument size. Besides, TMS is an in-hospital method requiring huge investment of time and money of the patients. In this respect, small size of the DBS electrodes can be attributed for its focused region of tissue activation, while magnetic stimulation can be credited for deep target tissue activation due to high permeability of magnetic field in biological tissues. It was Bonmassar *et al* [13] who had first shown the possibility of microscopic magnetic stimulation (*μ*MS) by using commercially available microcoils to stimulate deep brain target tissues. Later, his initiative led to customized fabrication of microcoils [14, 15], planar or solenoidal, giving effective and selective spatial control over the L5 pyramidal neurons [16], intracortical neurons [14] and inferior colliculus (IC) [17] neurons. However, the performance of these microcoils are limited by huge power consumption [13], increased thermal effects on gray matter [18] and lack of directionality (see figure 3 of [19]).

In 2016, Wang *et al* [20] filed a patent on the current driven motion of domain walls through a magnetic nanowire for neuron stimulation. In this paper, magnetic skyrmions in spintronic nanostructure for neuron stimulation have been proposed. It is shown that the time-varying magnetic field resulting from the dynamics of the skyrmions induces an electric field for neuron stimulation. Ever since the first experimental observation of skyrmions in 2009 [21], these topological structures have been believed to be of extensive use in the next generation neuromorphic computing, cutting-edge data processors and memory devices [22–24] and the topic has been subjected to extensive review [23, 25, 26]. The stability of skyrmions are facilitated by chiral exchange interaction and broken inversion symmetry that are inherent characteristics in bulk magnetic nanostructures or heavy metal/ferromagnetic metal (HM/FM) interfaces, of which the latter is energetically preferred [23]. Skyrmions, owing to their tiny dimension and topological stability, can be driven through magnetic multilayers with low threshold current [23], encouraging low power bio-inspired devices. Their velocity is directly proportional to the applied electrical current density [27] while it is remarkable how their dynamics can be controlled by defects [28], strength of magnetic field gradient and Gilbert damping constant [29]. Very recently, Pan *et al* [30] demonstrated a theoretical model for a skyrmion-based neuron recording system. This work proposes a skyrmion-based neurostimulator (SkyNS), a theoretical model of a spintronic neurostimulator being at nanometer scale facilitates cellular-level neurostimulation. The displacement of skyrmions on a HM/FM bilayer nanostructure results in time-domain change in magnetization along the device surface. Following Faraday's laws of electromagnetic induction, the time-rate of change of

magnetization over a specific area induces an electric field which can stimulate the neurons. SkyNS operates on a current of 2.71 *μ*A which is 10^3 times lower than the current consumed by magnetic microcoils and roughly of the same order when compared to DBS electrodes or microelectrodes used for electrical stimulation of neurons (see figure 4 of [15]). It is a proof-of-concept for the futuristic possibility of ultra-low power spintronic nanodevices as the next generation neurostimulators.

2. Skyrmion-based neurostimulator (SkyNS)

2.1. Physical model

The schematic view of SkyNS and its interface with the neurons is shown in figure 1(a). Region 1 of SkyNS contains an array of 12 Néel-type skyrmions (the effects of varying the number of skyrmions have been studied in the online supplementary information, S5 (stacks.iop.org/JPhysD/52/465002/mmedia)), each of diameter 20 nm (the effect of varying size of skyrmions have been studied in the supplementary information, S4). Passing charge current through the heavy metal (HM) causes spin accumulation along $\pm y$ and spin current along the z direction (see figure 1(b)). This drives the array of skyrmions through the ferromagnetic (FM) thin film from region 1 to region 2 by a phenomenon known as the spin Hall effect (SHE) across the HM/FM interface. The two regions are separated by a barrier with a higher perpendicular anisotropy constant (PMA) compared to the surrounding thin film for reasons explained in the section 3.3. Due to the movement of skyrmions from region 1 to region 2, the time-varying magnetizations are observed in both region 1 and region 2. Based on Faraday's law of electromagnetic induction, alternating magnetic flux density induces an electric field in regions 1 and 2:

$$\oint \boldsymbol{E} \cdot d\boldsymbol{l} = - \iint \frac{\partial \boldsymbol{B}}{\partial t} \cdot d\boldsymbol{S} \tag{1}$$

where $\boldsymbol{B}$ is the magnetic flux density, $\boldsymbol{E}$ is the induced electric field, $\boldsymbol{l}$ and S are the contour and the surface area of region 2 (or region 1), respectively. In this work, we will focus on the magnetization change along z direction ($\boldsymbol{M}_z$) and the corresponding induced electric field ($\boldsymbol{E}_z$) over region 2 exclusively for reasons elaborated in the supplementary information, S2 and S3.

2.2. Biological model

It has been known for a long time now that external neurostimulation can be achieved by applying an electric stimulus, either in the form of a voltage or in the form of a current. At the cellular level, application of this electric stimulus causes a change in ionic concentration through voltage-gated ion channels across the neuron cell membrane resulting in a change in voltage. This change in voltage across the neuron cell membrane generates the neuron action potential. However, for both types of electric stimulus, whether it is current or voltage, there exists a definite strength-duration relationship [31, 32] for the applied stimulus that determines whether the neuron cells will be activated or not. However, as for the case of
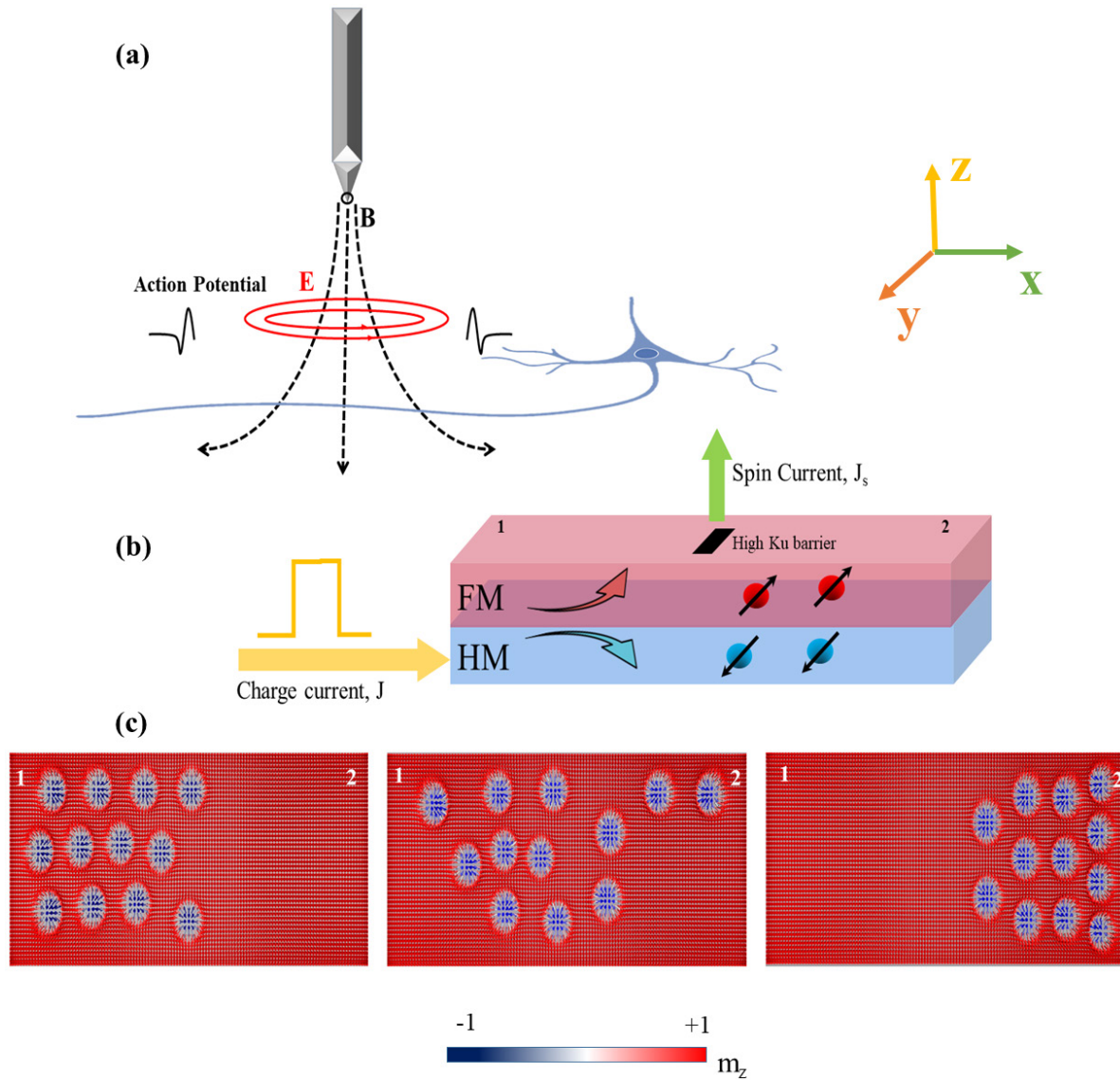
Figure 1. (a) Schematic view of the proposed tunable SkyNS mount on the tip of a stimulator probe and the device interface with the biological neurons. (b) The magnified image of the SkyNS at the tip of the probe. On applying a current through the HM, spin polarized electrons at the HM/FM interface cause the spin current to generate at a direction orthogonal to the device surface. A barrier of high perpendicular magnetic anisotropy (PMA) is situated in the center of the device dividing SkyNS into two regions: region 1 and region 2. (c) Snapshots of the top-view of the FM layer. The skyrmions nucleated in region 1, move due to effect of the spin current to region 2, bypassing the high PMA barrier. The displacement of skyrmions from region 1 to region 2 causes change in magnetization (M_z) of the FM layer which induces electric field that can stimulate nearby neurons by initiating two action potentials on the axon along two different directions: the orthodromic and antidromic. (Figure not to scale.)

SkyNS, to achieve neurostimulation through magnetic induction, the induced voltage which is proportional to the time derivative of the flux of the magnetic field, is presumed to satisfy the above strength-duration relationship for a voltage stimulus. But recent studies on neurostimulation have confirmed a third important parameter, which is frequency of the applied stimulus in addition to the strength and duration of the stimulus. The effect of this parameter has been better termed as repetitive magnetic stimulation (r-MS) [12, 15].

Studies have claimed that electrical stimulation by repetitive delivery or in ultrasound frequency can trigger neural responses even when the stimuli are of an amplitude lower than the threshold [33]. For instance, the threshold field strength for activation of hippocampal neurons are known [34] to be a single pulse of 10 V m^{-1} amplitude. But in 2003, Francis *et al*

[35] reported that an electric field strength of only 0.14 V m^{-1} is sufficient enough to stimulate hippocampal neurons if the frequency of stimuli delivery was within a range of 1–2 Hz. In other words, the threshold strength and duration for neurostimulation is significantly lowered when the frequency of the applied stimulus is increased [33]. A similar situation for micromagnetic neurostimulation was studied by Lee *et al* [15] on motor cortex of anesthetized mice where the movement of their whisker on implantation of microcoils would signify successful stimulation. It was experimentally determined that the lowest stimulation amplitude to trigger movement of whiskers by magnetic stimulation in anesthetized mice was only 11.2 mV (corresponding to a current of 0.75 mA through microcoil) for a frequency ranging from 1 Hz to 100 Hz; small stimulation amplitudes triggered small whisker movements

Parameters	Description	Values
Thin film dimension	Length $\times$ width $\times$ thickness	$500\,\text{nm} \times 200\,\text{nm} \times 1\,\text{nm}$
Cell size	Length $\times$ width $\times$ thickness	$2\,\text{nm} \times 2\,\text{nm} \times 1\,\text{nm}$
α	Gilbert damping factor	0.3
A	Exchange constant	$15 \times 10^{-12}\,\text{J}\,\text{m}^{-1}$
P	Spin Hall angle	0.4
M_s	Saturation magnetization	$580 \times 10^3\,\text{A}\,\text{m}^{-1}$
J	Electrical current density	$1 \times 10^{10}\,\text{A}\,\text{m}^{-2}$
μ_0	Permeability of free space	$4\pi \times 10^{-7}\,\text{Wb}\,\text{A}^{-1}\,\text{m}^{-1}$

and vice-versa. Although the possibility of r-MS in this form is encouraging, the long latency period for activation is the main challenge for microcoils.

The proposed SkyNS performs with a current pulse of 2.71 μA and can be easily tuned by varying the dimensions of the spintronic devices and/or barriers in the path of movement [36], the number of skyrmions [22] (also, see the supplementary information, S5), the applied electrical current density [22, 24, 27] (also, see the supplementary information, S6), introducing high anisotropy barrier acting as defect [22, 36] in the magnetic thin film and tuning the Dzyaloshinskii–Moriya interaction (DMI) until a stable skyrmion is nucleated [36, 37]. For SkyNS, on applying a charge current to the HM, it causes displacement of the skyrmions along the magnetic thin film which results in a change in magnetic flux along the device surface, inducing an electric field to trigger neurostimulation. It has been explained in section 3 how the strength, duration and frequency of the stimulus for neurostimulation from SkyNS can be efficiently tuned by magnetic material properties and device dimensions.

2.3. Micromagnetic simulations

Mumax3 [38] along with a DMI module was used to perform the 3D micromagnetic simulations. The average energy density calculations include the exchange energy, the anisotropy energy, the applied field (Zeeman) energy, the magnetostatic (demagnetization) energy and the DMI energy terms. SkyNS has been numerically simulated based on the Landau–Lifshitz–Gilbert (LLG) equation with a spin orbit torque (SOT) term as follows [22]:

$$\frac{d\boldsymbol{m}}{dt} = \gamma_0 \boldsymbol{h}_{\text{eff}} \times \boldsymbol{m} + \alpha \boldsymbol{m} \times \frac{d\boldsymbol{m}}{dt} + \frac{u}{t}\boldsymbol{m} \times (\boldsymbol{m}_{\text{p}} \times \boldsymbol{m}) \quad (2)$$

where $\boldsymbol{m} = \boldsymbol{M}/M_s$ is the normalized magnetization, $\gamma_0 = -2.211 \times 10^5\,\text{mA}^{-1}\,\text{s}^{-1}$ is the gyromagnetic ratio, $\boldsymbol{h}_{\text{eff}} = \boldsymbol{H}_{\text{eff}}/M_s$ is the reduced effective field, t is the thickness of the FM layer, $\boldsymbol{m}_{\text{p}}$ is the current polarization vector, $u = \gamma_0 \left(\frac{\hbar j P}{2 e M_s} \right)$, and j is the density of the spin current. The values of parameters M_s, P, α along with dimensions of the magnetic thin film are listed in table 1. All parameters are adopted from [39], for $t = 0.4\,\text{nm}$ thick Co (FM) layer on Pt (HM) layer.

The dimension of the magnetic thin film is set as $500\,\text{nm} \times 200\,\text{nm} \times 1\,\text{nm}$. All models are discretized into cells

with sizes of $2\,\text{nm} \times 2\,\text{nm} \times 1\,\text{nm}$ in the simulation which is sufficiently smaller than the skyrmion diameter (20 nm) which guarantees numerical precision along with computational efficiency. The run time of the simulation is fixed at 200 ns. All other parameters used in this work are listed in table 1. The initial magnetic states of the thin film are relaxed along the $+z$ direction, except for the tilted magnetization near the edges due to the DMI. Initially, an array of 12 skyrmions are nucleated in region 1 of the magnetic thin film at desired positions, 60 nm apart from each other as shown in figure 1(c). Then they are moved from region 1 to region 2 by the transverse spin-polarized current and then relaxed to stable/metastable state within a short period of time.

The skyrmion dynamics can be explained by the Thiele equation [36]:

$$\boldsymbol{G} \times \left(\boldsymbol{v}^s - \boldsymbol{v}^d \right) - D\alpha \boldsymbol{v}^d - \boldsymbol{F}(x) = 0 \quad (3)$$

where D is the magnitude of DMI, $\boldsymbol{v}^d$ is the drift velocity of the skyrmions, $\boldsymbol{v}^s$ is the velocity induced by spin current. $G = (0, 0, 4\pi Q)$ is the gyromagnetic coupling vector representing the Magnus force, Q is the topological winding number of the skyrmion given by, $Q = -\int dx \frac{1}{4\pi} \boldsymbol{m}(\boldsymbol{x}) \cdot (\partial_x \boldsymbol{m}(\boldsymbol{x}) \times \partial_y \boldsymbol{m}(\boldsymbol{x}))$, and $F(x) = \nabla V(x)$ is the force induced by skyrmion potential. The potential is given by the local energy of a skyrmion [36]:

$$E_{\text{sk}} = -\frac{D^2 \pi^4}{4K\pi + \frac{16}{\pi}B} + 38.7A \quad (4)$$

where B is the magnetic flux density (here, $B = \mu_0 M$), A is the exchange constant, K is the anisotropic energy of the film (here, for barrier (Ku_b) and for the surrounding thin film (Ku_s)). Evidently, from equation (4) high DMI, high exchange constant, low anisotropy and a low magnetic flux density independently contributes to high energy skyrmions. Also, the radius of the nucleated skyrmion is given by [36]:

$$R_{\text{sk}} = -\frac{D\pi^2}{2K\pi + \frac{8}{\pi}B}. \quad (5)$$

The values of parameters are listed in table 1. Therefore, from equation (5) a high DMI, a low anisotropy and a low magnetic flux density independently contributes to increased radius of the skyrmion. The tuning of these parameters to suffice our therapeutic application will be discussed in the section 3 where it has been observed that high energy and large skyrmion size often results in an unstable skyrmionic system.
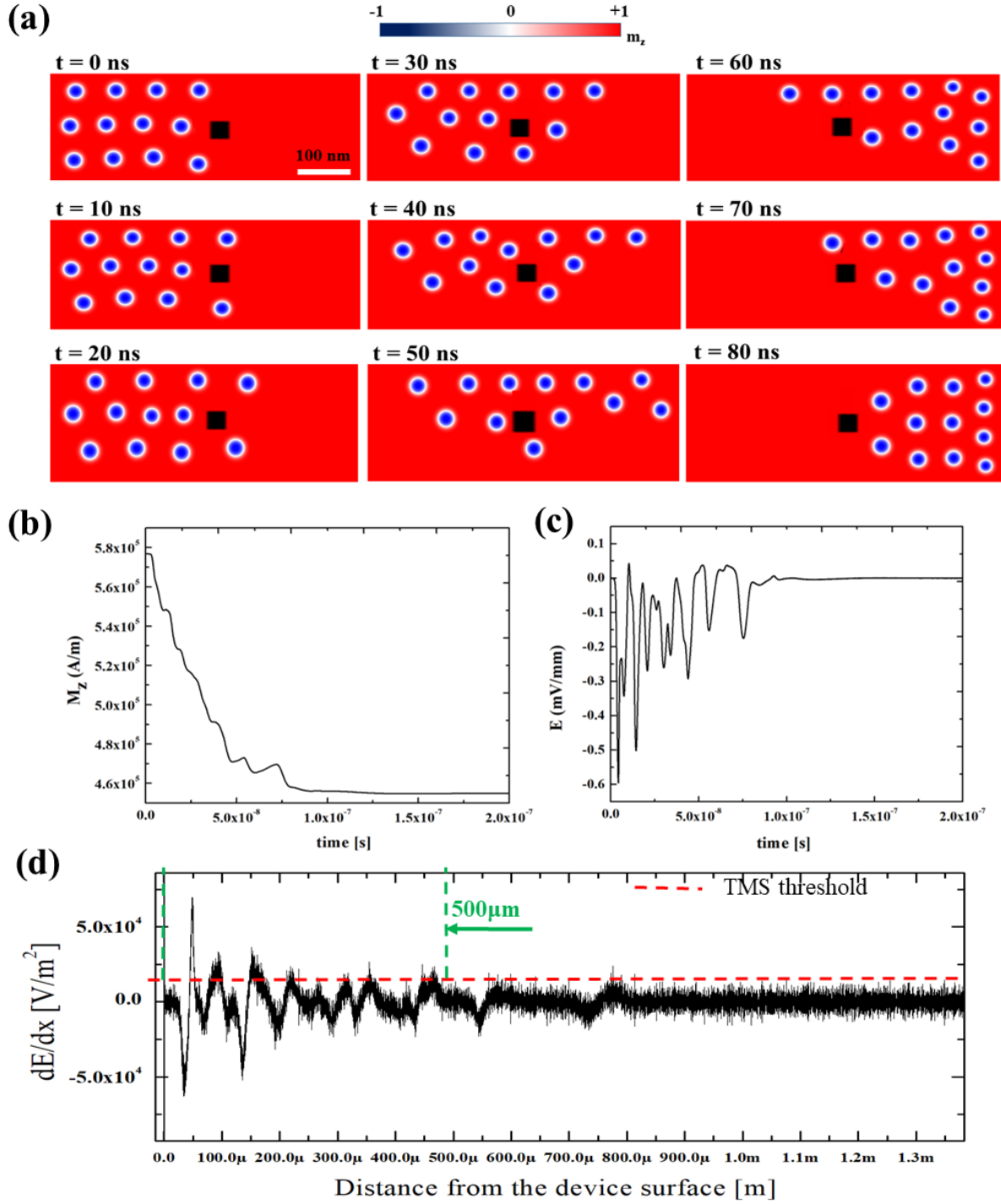
J. Phys. D: Appl. Phys. **52** (2019) 465002

R Saha *et al*

Figure 2. (a) Spatial distribution of magnetization at a time step of 10 ns for an array of 12 skyrmions moving across a HM/FM thin film bypassing the barrier from region 1 to region 2 for single pulse of charge current, $J = 1 \times 10^{10}$ A m^{-2} of duration 200 ns. The color scale shows the out-of-plane magnetization, m_z. The skyrmionic dynamics in magnetic thin film for this case can be found in supplementary movie SM1. (b) The time-resolved out-of-plane magnetization (the magnetization component along the z direction) in region 2 of the magnetic thin film for a single current pulse of 200 ns. (c) The induced electric field over region 2 as a function of time for a single current pulse of 200 ns. (d) The plot of electric field gradient over 1.3 mm above the thin film surface of region 2 where the neurons will be present. It is seen that the electric field exceeds the TMS threshold up to 500 μm away from the device surface. The device operation paves the way for selective activation of neurons based on its location up to 500 μm away from the surface.

J. Phys. D: Appl. Phys. **52** (2019) 465002

R Saha *et al*

3. Results and discussion

3.1. Current driven movement of skyrmions and the induced electric field from SkyNS

On applying an electric current density $J = 1 \times 10^{10} \, \text{A} \, \text{m}^{-2}$ to the HM, the spin polarized current driven motion of the nucleated skyrmions have been observed in presence of a barrier with PMA value higher than the surroundings, i.e. $\text{Ku}_\text{b} > \text{Ku}_\text{s}$. Figure 2(a) gives the simulated snapshots at a time step of 10 ns showing the skyrmions nucleated with $\text{DMI} = 3 \, \text{mJ} \, \text{m}^{-2}$ in motion. The skyrmions move past the barrier with dimensions, $y_\text{b} \times x_\text{b} = 40 \, \text{nm} \times 40 \, \text{nm}$ and PMA constant, $\text{Ku}_\text{b} = 0.84 \, \text{MJ} \, \text{m}^{-3}$, while the surrounding thin film has $\text{Ku}_\text{s} = 0.7 \, \text{MJ} \, \text{m}^{-3}$. The magnetization over region 2 changes over a time duration of ~80 ns (see figure 2(b)), so does the induced electric field over region 2 (see figure 2(c)); both for a single pulse current of duration 200 ns. The corresponding electric field gradient at a distance from the magnetic thin film surface is demonstrated in the 2D electric field gradient plot in figure 2(d) which implies that the electric field gradient exceeds the TMS threshold [15] of 11 000 V m^{-2} at multiple distances up to a distance of 500 μm above the magnetic thin film surface. This implies that only at those points if the neurons are present, they are activated. The remaining points where it does not cross the threshold, the neurons are not activated. This gives SkyNS an added advantage over the magnetic stimulation methods in [15, 40] as it paves the way for selective activation of neurons at selective distances from the surface of SkyNS within 500 μm range. Furthermore, the performance of magnetic neurostimulation from SkyNS is better than the custom fabricated microcoils demonstrated in [15] which are not only limited by large dimension (~100 μm) but also has an effective electric field gradient over a distance of only 60–75 μm from the device surface [15]. The discussion in the following sections are focused on how to further improve the performance of SkyNS.

In figure 2(a), only a single pulse of current of duration 200 ns is applied. But from our simulations it is seen that all skyrmions can reach region 2 from region 1 within 80 ns (see figure 2(b)). Again, after 80 ns, if another charge current density of same magnitude and duration but different direction is passed through the HM, the skyrmions will pass from region 2 to region 1 similar to what demonstrated in the device operation in [22]. Then, this time, region 1 will yield the induced electric field for neurostimulation and the operation will repeat depending up on the charge current duration and direction. The frequency at which the direction of the charge current is altered will be the frequency of r-MS. However, for all the following cases to maintain uniformity to explain the device operation of SkyNS, only a single pulse of current of duration 200 ns has been considered.

3.2. Tuning the combinations of DMI and Ku$_\text{s}$/Ku$_\text{b}$ ratio of the SkyNS

Figure 3 shows a working window for the magnetization patterns of the magnetic thin films with identical barrier

dimensions, $y_\text{b} \times x_\text{b} = 40 \, \text{nm} \times 40 \, \text{nm}$ at run-time, $t = 200 \, \text{ns}$ but for different combinations of DMI and Ku$_\text{s}$/Ku$_\text{b}$ ratios. These different combinations of magnetic parameters are tuned to study their effect on the stable nucleation of skyrmions and their smooth movement through the thin film into region 2. Experimentally, magnetic anisotropy can be tuned by ion irradiation and DMI strength can be reduced by increasing the film thickness [37].

Three distinct characteristics of the working window have been observed: (i) along the diagonal, for the cases where $\text{DMI} = 2.5 \, \text{mJ} \, \text{m}^{-2}, \text{Ku}_\text{s}/\text{Ku}_\text{b} = 0.8$ and for $\text{DMI} = 3 \, \text{mJ} \, \text{m}^{-2}, \text{Ku}_\text{s}/\text{Ku}_\text{b} = 1$ satisfy both requirements for stable nucleation of skyrmions and imply smooth movement bypassing the barrier. For the remaining cases along the diagonal, when $\text{Ku}_\text{b} > \text{Ku}_\text{s}$, the DMI effect is more prominent over the PMA ratio effect which corresponds to formation of larger skyrmions as it follows from equation (5). For $\text{Ku}_\text{b} < \text{Ku}_\text{s}$ along the diagonal, the skyrmions enter the lower Ku barrier region from a higher Ku surrounding film and get trapped in the barrier before moving to region 2 which has been discussed in detail in section 3.3. (ii) Beneath the diagonal, the DMI values are very small. Hence, the skyrmions nucleate with smaller radii which agrees with equation (5). For the case where the $\text{DMI} = 2 \, \text{mJ} \, \text{m}^{-2}, \text{Ku}_\text{s}/\text{Ku}_\text{b} = 0.8$, the energy from equation (4) is just enough to nucleate skyrmions. This leads to the annihilation of skyrmions immediately after their nucleation (see supplementary movie SM2). For the remaining cases below the diagonal, the combinations of DMI and Ku$_\text{s}$/Ku$_\text{b}$ values lead to low energy of the skyrmions which is insufficient for the skyrmion nucleation as it follows directly from equation (4). (iii) Above the diagonal, the large DMI values increase both the energy as well as the radius of the skyrmions above the threshold, leading to the formation of elongated Néel stripes [41]. They nucleate fast and spread all over the magnetic thin film, causing a huge change of magnetization throughout the entire thin film. Such a condition is referred to as the elliptical instability [42]. But they remain static at their position of nucleation, even after application current pulse, which implies there is little change in time duration. Thus, there will be no induced electric field to stimulate the neurons. The video for the case of $\text{DMI} = 4 \, \text{mJ} \, \text{m}^{-2}, \text{Ku}_\text{s}/\text{Ku}_\text{b} = 0.6$ for $t = 200 \, \text{ns}$ is attached in supplementary movie SM3.

In summary, figure 3 provides the combinations, $\text{DMI} = 3 \, \text{mJ} \, \text{m}^{-2}, \text{Ku}_\text{s}/\text{Ku}_\text{b} = 1$ and $\text{DMI} = 2.5 \, \text{mJ} \, \text{m}^{-2}, \text{Ku}_\text{s}/\text{Ku}_\text{b} = 0.8$, that are energetically favorable for stable skyrmion nucleation in region 1 and smooth movement bypassing the barrier to region 2.

3.3. Tuning the combination of Ku$_\text{s}$/Ku$_\text{b}$ and y_b/x_b ratios of SkyNS

The working window in figure 4 demonstrates the snapshots of the magnetic thin film with $\text{DMI} = 3 \, \text{mJ} \, \text{m}^{-2}$ (a value chosen from the best device performance in figure 3) at $t = 200 \, \text{ns}$ with varying PMA ratios of the barrier to the surroundings and varying aspect ratios of the barrier in the nanodevice.
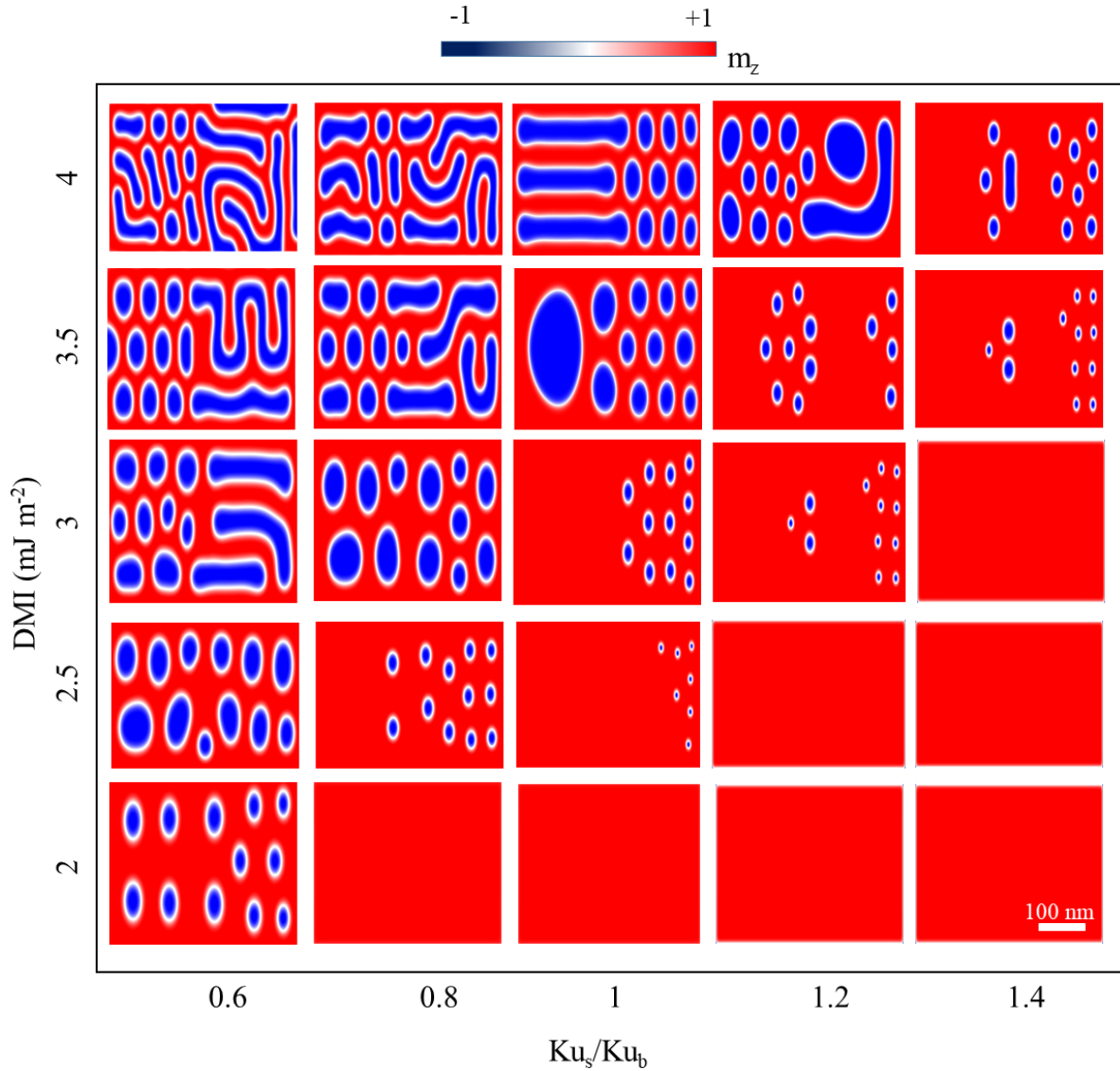
Figure 3. Snapshots of region 2 of SkyNS at $t = 200$ ns. The working window of the movement of skyrmions to region 2 under different combinations of DMI and Ku_s/Ku_b, the barrier dimension is identical $y_b \times x_b = 40$ nm $\times$ 40 nm and is positioned in the center the nanodevice. The requirements for neuron stimulation are best satisfied along the diagonal of the window for cases where DMI $= 2.5$ mJ m^{-2}, $Ku_s/Ku_b = 0.8$ and DMI $= 3$ mJ m^{-2}, $Ku_s/Ku_b = 1$. This confirms that for smooth movement of skyrmions, Ku_b must preferably be greater than or equal to Ku_s. Below the diagonal in that window, the skyrmions are either nucleated in smaller diameters (for cases where DMI $= 2.5$ mJ m^{-2}, $Ku_s/Ku_b = 1$; DMI $= 3$ mJ m^{-2}, $Ku_s/Ku_b = 1.2$ and DMI $= 3.5$ mJ m^{-2}, $Ku_s/Ku_b = 1.4$) or annihilate immediately after their nucleation (for DMI $= 2$ mJ m^{-2}, $Ku_s/Ku_b = 0.8$, see supplementary movie SM2) or like the remaining cases below the diagonal where skyrmions never nucleate. For cases above the diagonal, they form elongated Néel stripes which induces negligible electric field unsuitable for our application in neuron stimulation (for DMI $= 4$ mJ m^{-2}, $Ku_s/Ku_b = 0.6$, see supplementary movie SM3). The color scale shows the out-of-plane magnetization, m_z.

The results of the working window in figure 4 are concluded as follows: (i) for $Ku_b = Ku_s$, under any y_b/x_b ratio, the skyrmions face no barrier in their path of movement. Hence, all skyrmions reach region 2 and, as expected, show a huge change in magnetization implying a strong induced electric field (see figure 5(a) and (b) for $Ku_s/Ku_b = 1$). (ii) For $Ku_b < Ku_s$, the barrier acts as a sink. In this case, when $y_b < x_b$, most of the skyrmions bypass the barrier to region 2, a few skyrmions still remain trapped in the low Ku barrier. Interestingly, when $y_b > x_b$, the skyrmions that were trapped in the low Ku barrier act as a barrier to the remaining

skyrmions. This also explains why few skyrmions for some of the cases below the diagonal of the working window in figure 3 did not reach region 2. The change in magnetization in region 2 is therefore negligible, so is the induced electric field essential for neurostimulation (see figures 5(a) and (b) for $Ku_s/Ku_b = 1.2$ & 1.4). (iii) For $Ku_b > Ku_s$, the barrier of higher Ku acts as a hurdle in the path of skyrmion movement causing the skyrmions to bypass the barrier. As y_b becomes larger than x_b, within a time window of 200 ns, it is observed that fewer skyrmions arrive at region 2. Thus, although the change in magnetization over region 2 in this case would be
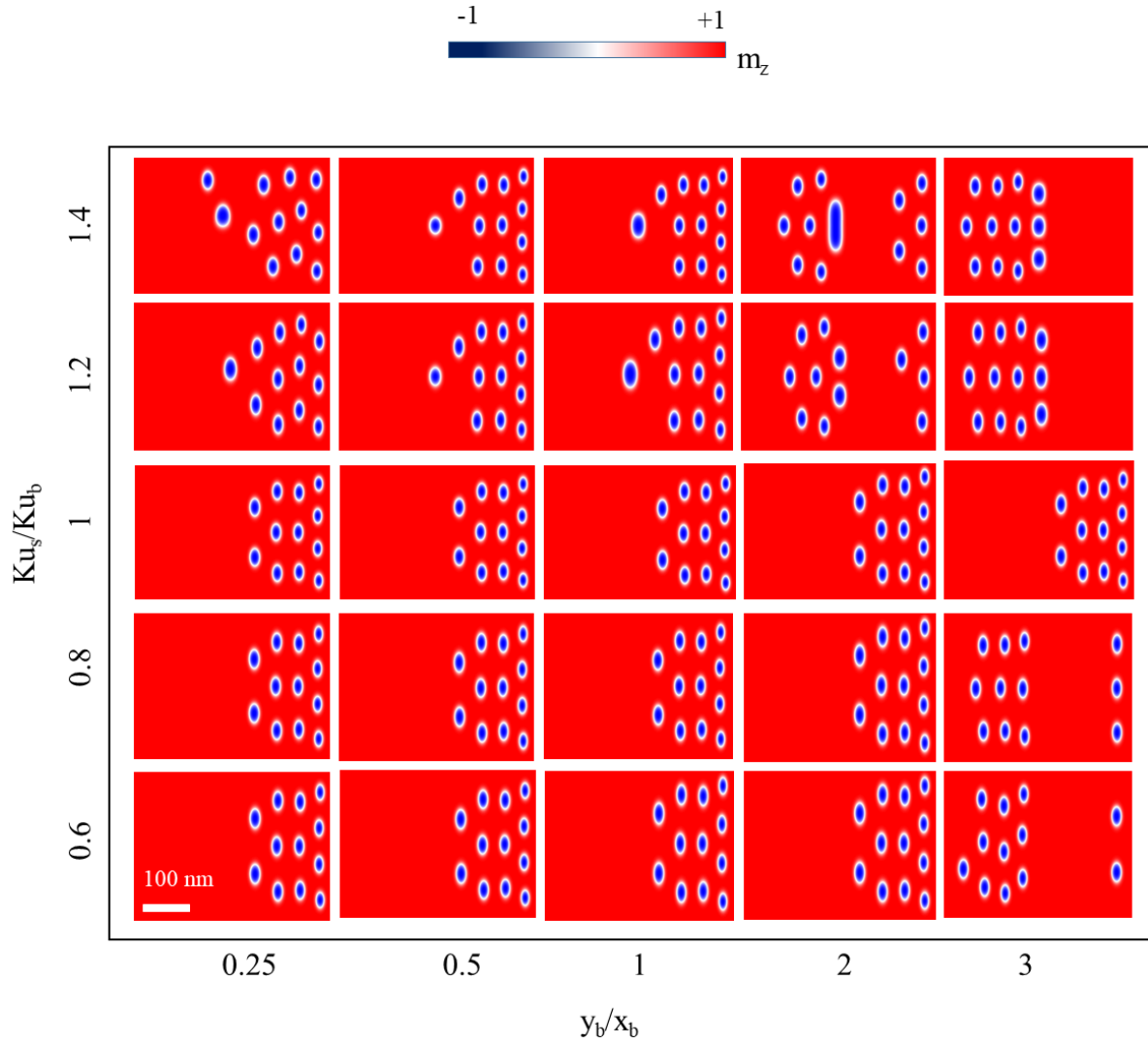
Figure 4. Snapshot of region 2 of SkyNS at $t = 200$ ns. The working window for different combinations of Ku_s/Ku_b and y_b/x_b of the nanodevice. The barrier has a position central to the nanodevice. (i) When $Ku_b = Ku_s$, the skyrmions face no barrier in their path of movement. (ii) When $Ku_b < Ku_s$, the barrier acts as a sink. (iii) When $Ku_b > Ku_s$, the barrier acts as a hurdle in the path of skyrmion movement, delaying the skyrmions. The color scale shows the out-of-plane magnetization, m_z.

smaller than the case where $Ku_s = Ku_b$, the time duration for change in magnetization would be higher. This implies the induced electric field will persist over a longer duration of time (see figure 5(a) and (b) for $Ku_s/Ku_b = 0.6$ & 0.8) which is a win–win situation for neurostimulation.

It is worth mentioning here that $y_b > x_b$ affects the dynamics of skyrmions whereas the cases for $y_b < x_b$ affect the number of skyrmion nucleation. This is because the alignments of the array of skyrmions are different in region 1 (see figure 2(a)) compared to that when they arrive in region 2. At $t = 0$ ns in figure 2(a), the 12 skyrmions are arranged in region 1 with greater number of skyrmions along the x-axes. On the contrary, when the skyrmions bypass the barrier in to region 2, the skyrmions are arranged in region 2 with a greater number of skyrmions along the y-axes than along the x-axes. For $y_b \gg x_b$ i.e. when the length of y_b is comparable to the width of the thin film (which in this manuscript is 200 nm), then the skyrmions will face difficulty in bypassing the barrier and reach region 2. For instance, the cases where (i)

$y_b/x_b = 3$, $Ku_s/Ku_b = 0.8$ and (ii) $y_b/x_b = 3$, $Ku_s/Ku_b = 0.6$ in figure 4. As $Ku_b > Ku_s$ in both cases, the skyrmions do not have the possibility to sink into the barrier. But still, only three skyrmions in case (i) and only two skyrmions in case (ii) reach region 2 within a run time of 200 ns. This implies that when $y_b \gg x_b$, it delays the skyrmions thereby affecting the skyrmion dynamics. On the other hand, if $y_b < x_b$, the 12 skyrmions will not have enough space in the magnetic thin film to nucleate in region 1 at all. If a smaller number of skyrmions are nucleated, then a smaller number of skyrmions arrive in region 2 implying smaller duration in which magnetization persists over region 2 which directly follows a lower duration of induced electric field for neurostimulation. The effect of the number of skyrmions on neurostimulation has been demonstrated in supporting information S5.

In summary, the barrier plays the same role as that of the edge states at the film boundaries that keeps skyrmions inside. Furthermore, our results indicate that the lateral size of such a barrier (y_b) must also be small enough that skyrmions pass
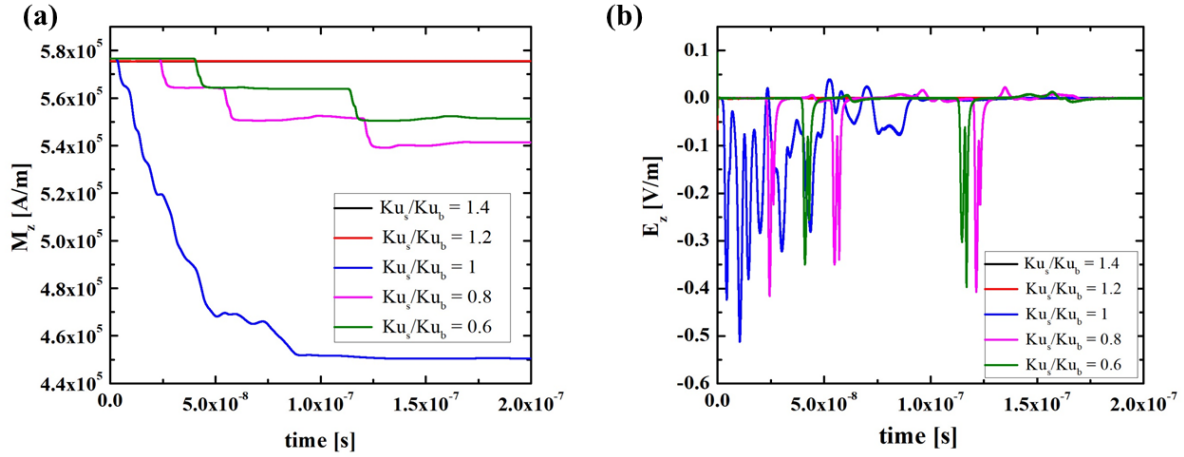
Figure 5. (a) The time-resolved out-of-plane magnetization, $M_z (= m_z * M_s)$ in region 2 of the magnetic thin film for a single current pulse of 200 ns for $y_b/x_b = 3$. (b) The induced electric field over region 2 for $y_b/x_b = 3$ as a function of time for a single current pulse of 200 ns. For $Ku_s > Ku_b$, there is no change in magnetization and hence no induced electric field over region 2. When $Ku_s = Ku_b$, a huge change in magnetization induces a strong electric field over region 2. However, the most satisfactory conditions for neuron stimulation are when $Ku_s < Ku_b$. In this case, although the strength of the induced electric field over region 2 reduces slightly, the time duration through which the induced electric field will persist for neuron stimulation, increases significantly.

Table 2. Calculation of energy consumption and area overhead.

Parameters	Description	Values
Thin film dimension	Length × width × thickness	$500\,nm \times 200\,nm \times 1\,nm$
J	Electrical current density	$1 \times 10^{10}\,A\,m^{-2}$
Area of HM	Width × thickness	$200\,nm \times 0.6\,nm$
Area of FM	Width × thickness	$200\,nm \times 0.4\,nm$
ρ_{Pt}	Resistivity of HM	10.6×10^{-8} Ohm m
R_{Pt}	Resistance of HM	441.6 Ohm
ρ_{Co}	Resistivity of FM	5.6×10^{-8} Ohm m
R_{Co}	Resistance of FM	350 ohm
R_{eq}	Equivalent resistance	195.26 Ohm
I	Total current	2.71 μA
P	Power consumption	1.434 nW

over it due to the skyrmion Hall effect while being driven by the spin-polarized current.

3.4. Power consumption and device performance

To confirm the better power efficiency of SkyNS as a spintronic nanodevice over its CMOS analogues, the total power consumption and area overhead are calculated and listed in table 2. The HM/FM layers have been considered to have resistances in parallel. The terms current density (J, Am^{-2}) refers to current through the HM only. The total current (I, μA) refers to the current through the entire device. SkyNS has a power efficiency which is calculated by the product of square of the total current to SkyNS and the equivalent resistance of the HM/FM bilayer. Considering the average motion duration of the skyrmions in the nanodevice to be 200 ns, the power consumption of SkyNS were calculated as 1.434 nW which is about 10^{16} times lower than commercialized TMS coils (owing to its bulky dimension) and 10^6 times lower than DBS electrodes [15, 43]. Although implantable magnetic microcoils have shown significant improvements in levels

of power consumption over the years through use of fabricated microcoils [15] instead of the first-generation inductors [13] as neurostimulators, they still consume about 10^4 times more power than SkyNS. In short, SkyNS promises the lowest reported power consumption for implantable neurostimulators till date (see figure S1 in the supplementary information, S1). These calculations strongly encourage the use of implantable spintronic neurostimulators for miniaturization of power consumption.

4. Conclusions

To conclude, we have proposed a highly tunable, implantable, skyrmion-based micromagnetic neurostimulator, SkyNS, that operates at a current of 2.71 μA and at a power of only 1.434 nW thereby minimizing thermal effects on gray matter significantly. The device dimensions being of the order of several nanometers which is much smaller than the average size of a neuron (0.004 mm to 0.1 mm), SkyNS shows the potential of focally stimulating single neurons. This is a property which is lacking in the existing neurostimulators

due to their relatively large dimension (see table 1 of [44]). The value of $DMI = 3\,mJ\,m^{-2}$ is advantageous for stable skyrmion nucleation. DMI values higher than this nucleates elongated Néel stripes while lower DMI value nucleates low energy skyrmions which annihilates immediately after nucleation. A barrier which is situated in the center of the HM/FM bilayer should preferably have a PMA value higher than the surrounding thin film to facilitate smooth movement of all skyrmions from region 1 to region 2. It is extremely necessary that all the nucleated skyrmions reach region 2 as this would cause a suitable change in magnetization over region 2 implying a greater value of induced electric field to stimulate the neurons. The size of the skyrmions has little to no effect on the therapeutic performance of SkyNS. However, our simulation studies show that the number of skyrmions nucleated do influence the device performance to a certain extent. As SkyNS magnetically stimulates neurons, in addition to the strength of the induced electric field, the time duration for which the induced electric field persists for a single current pulse applied is also a factor to be considered carefully. Our results indicate that the lateral dimension of the high Ku barrier is the deciding factor for the number of skyrmions reaching region 2 and the time duration through which the change in magnetization over region 2 takes place. The greater the lateral dimension of the barrier, the fewer skyrmions reach region 2 implying smaller change in magnetization over region 2 and hence the strength of the induced electric field will also be lower. But a higher lateral dimension of the barrier also slows down the skyrmions which causes the change in magnetization and hence the induced electric field to persist for a longer duration of time over region 2. Therefore, the lateral size of the barrier must be small enough to allow the skyrmions to bypass the barrier into region 2. It is also observed that when a lower Ku barrier is employed, the skyrmions get trapped in the barrier and do not reach region 2 at all. Despite the fact that the nucleation, stabilization and manipulation of a group of skyrmions in and along defects have been analytically predicted earlier [22, 37], the perfect controlling of those nucleated skyrmions in a magnetic thin film such that they can meet the therapeutic specifications of a neuron stimulating device has been the primary focus of this work. Spintronic-based SkyNS shows a promising future for low power implantable magnetic neurostimulators.

Acknowledgments

Notes

The authors declare no conflict of interest.

ORCID iDs

Renata Saha ● https://orcid.org/0000-0002-0389-0083
Kai Wu ● https://orcid.org/0000-0002-9444-6112
Diqing Su ● https://orcid.org/0000-0002-5790-8744
Jian-Ping Wang ● https://orcid.org/0000-0003-2815-6624

References

[1] Amon A and Alesch F 2017 Systems for deep brain stimulation: review of technical features *J. Neural Transm.* **124** 1083–91
[2] Tjong F V Y and Reddy V Y 2017 Permanent leadless cardiac pacemaker therapy: a comprehensive review *Circulation* **135** 1458–70
[3] Nguyen S, Cloutier F, Philippon D, Côté M, Bussieres R and Backous D D 2016 Outcomes review of modern hearing preservation technique in cochlear implant *Auris Nasus Larynx* **43** 485–8
[4] Hafner B J, Gaunaurd I A, Morgan S J, Amtmann D, Salem R and Gailey R S 2017 Construct validity of the Prosthetic Limb Users Survey of Mobility (PLUS-M) in adults with lower limb amputation *Arch. Phys. Med. Rehabil.* **98** 277–85
[5] Weiland J D, Cho A K and Humayun M S 2011 Retinal prostheses: current clinical results and future needs *Ophthalmology* **118** 2227–37
[6] Golestanirad L, Kirsch J, Bonmassar G, Downs S, Elahi B, Martin A, Iacono M-I, Angelone L M, Keil B and Wald L L 2019 RF-induced heating in tissue near bilateral DBS implants during MRI at 1.5 T and 3T: the role of surgical lead management *NeuroImage* **184** 566–76
[7] Rezai A R, Phillips M, Baker K B, Sharan A D, Nyenhuis J, Tkach J, Henderson J and Shellock F G 2004 Neurostimulation system used for deep brain stimulation (DBS): MR safety issues and implications of failing to follow safety recommendations *Investig. Radiol.* **39** 300–3
[8] Iacono M I, Makris N, Mainardi L, Angelone L M and Bonmassar G 2013 MRI-based multiscale model for electromagnetic analysis in the human head with implanted DBS *Comput. Math. Methods Med.* **2013** 694171
[9] Skousen J L, Bridge M J and Tresco P A 2015 A strategy to passively reduce neuroinflammation surrounding devices implanted chronically in brain tissue by manipulating device surface permeability *Biomaterials* **36** 33–43
[10] Polikov V S, Tresco P A and Reichert W M 2005 Response of brain tissue to chronically implanted neural electrodes *J. Neurosci. Methods* **148** 1–18
[11] Brunoni A R, Chaimani A, Moffa A H, Razza L B, Gattaz W F, Daskalakis Z J and Carvalho A F 2017 Repetitive transcranial magnetic stimulation for the acute treatment of major depressive episodes: a systematic review with network meta-analysis *JAMA Psychiatry* **74** 143–52
[12] Galhardoni R, Correia G S, Araujo H, Yeng L T, Fernandes D T, Kaziyama H H, Marcolin M A, Bouhassira D, Teixeira M J and de Andrade D C 2015 Repetitive transcranial magnetic stimulation in chronic

J. Phys. D: Appl. Phys. 52 (2019) 465002

R Saha *et al*

pain: a review of the literature *Arch. Phys. Med. Rehabil.* **96** S156–S72

[13] Bonmassar G, Lee S W, Freeman D K, Polasek M, Fried S I and Gale J T 2012 Microscopic magnetic stimulation of neural tissue *Nat. Commun.* **3** 921

[14] Lee S W, Thyagarajan K and Fried S 2018 Micro-coil design influences the spatial extent of responses to intracortical magnetic stimulation *IEEE Trans. Biomed. Eng.* **66** 1680–94

[15] Lee S W, Fallegger F, Casse B D F and Fried S I 2016 Implantable microcoils for intracortical magnetic stimulation *Sci. Adv.* **2** e1600889

[16] Lee S W and Fried S I 2014 The response of L5 pyramidal neurons of the PFC to magnetic simulation from a micro-coil *36th Annual Int. Conf. IEEE Engineering in Medicine and Biology Society* (IEEE) pp 6125–8

[17] Park H-J, Bonmassar G, Kaltenbach J A, Machado A G, Manzoor N F and Gale J T 2013 Activation of the central nervous system induced by micro-magnetic stimulation *Nat. Commun.* **4** 2463

[18] Park H-J, Seol J H, Ku J and Kim S 2015 Computational study on the thermal effects of implantable magnetic stimulation based on planar coils *IEEE Trans. Biomed. Eng.* **63** 158–67

[19] Golestanirad L, Gale J T, Manzoor N F, Park H-J, Glait L, Haer F, Kaltenbach J A and Bonmassar G 2018 Solenoidal micromagnetic stimulation enables activation of axons with specific orientation *Frontiers Psychol.* **9** 724

[20] Wang J-P, Low W C and Mahendra D C 2016 Magnetic nanostimulator and nanosensor array for biological material stimulation and sensing *Google Patents*

[21] Mühlbauer S, Binz B, Jonietz F, Pfleiderer C, Rosch A, Neubauer A, Georgii R and Böni P 2009 Skyrmion lattice in a chiral magnet *Science* **323** 915–9

[22] Huang Y, Kang W, Zhang X, Zhou Y and Zhao W 2017 Magnetic skyrmion-based synaptic devices *Nanotechnology* **28** 08LT2

[23] Jiang W, Chen G, Liu K, Zang J, te Velthuis S G E and Hoffmann A 2017 Skyrmions in magnetic multilayers *Phys. Rep.* **704** 1–49

[24] He Z and Fan D 2017 A tunable magnetic skyrmion neuron cluster for energy efficient artificial neural network *Design, Automation and Test in Europe Conf. Exhibition* (IEEE) pp 350–5

[25] Fert A, Reyren N and Cros V 2017 Magnetic skyrmions: advances in physics and potential applications *Nat. Rev. Mater.* **2** 17031

[26] Kang W, Huang Y, Zhang X, Zhou Y and Zhao W 2016 Skyrmion-electronics: an overview and outlook *Proc. IEEE* **104** 2040–61

[27] Iwasaki J, Mochizuki M and Nagaosa N 2013 Universal current-velocity relation of skyrmion motion in chiral magnets *Nat. Commun.* **4** 1463

[28] Hanneken C, Kubetzka A, Von Bergmann K and Wiesendanger R 2016 Pinning and movement of individual nanoscale magnetic skyrmions via defects *New J. Phys.* **18** 055009

[29] Wang C, Xiao D, Chen X, Zhou Y and Liu Y 2017 Manipulating and trapping skyrmions by magnetic field gradients *New J. Phys.* **19** 083008

[30] Pan B, Wang K, Chen X, Bai J, Yang J, Li S, Zhang Y and Zhao W 2019 Magnetic skyrmion-based neural recording system design for brain-machine interface *IEEE Int. Symp. Circuits and Systems (ISCAS)* (IEEE) pp 1–5

[31] Geddes L A and Bourland J D 1985 The strength-duration curve *IEEE Trans. Biomed. Eng.* **BME-32** 458–9

[32] Rogers W R, Merritt J H, Comeaux J A, Kuhnel C T, Moreland D F, Teltschik D G, Lucas J H and Murphy M R 2004 Strength-duration curve for an electrically excitable tissue extended down to near 1 nanosecond *IEEE Trans. Plasma Sci.* **32** 1587–99

[33] Lin C-W, Lin M-L, Lu S-S, Shih W-P, Wen Y-R and Chiu H-W 2011 Implantable pulsed-radiofrequency micro-stimulation system *Google Patents*

[34] Chan C Y and Nicholson C 1986 Modulation by applied electric fields of Purkinje and stellate cell activity in the isolated turtle cerebellum *J. Physiol.* **371** 89–114

[35] Francis J T, Gluckman B J and Schiff S J 2003 Sensitivity of neurons to weak electric fields *J. Neurosci.* **23** 7255–61

[36] Zhang X, Zhou Y, Ezawa M, Zhao G P and Zhao W 2015 Magnetic skyrmion transistor: skyrmion motion in a voltage-gated nanotrack *Sci. Rep.* **5** 11369

[37] Sampaio J, Cros V, Rohart S, Thiaville A and Fert A 2013 Nucleation, stability and current-induced motion of isolated magnetic skyrmions in nanostructures *Nat. Nanotechnol.* **8** 839

[38] Vansteenkiste A, Leliaert J, Dvornik M, Garcia-Sanchez F and Van Waeyenberge B 2014 The design and verification of mumax3 *AIP Adv.* **4** 107133

[39] Wiesendanger R 2016 Nanoscale magnetic skyrmions in metallic films and multilayers: a new twist for spintronics *Nat. Rev. Mater.* **1** 16044

[40] Maccabee P J, Amassian V E, Eberle L P and Cracco R Q 1993 Magnetic coil stimulation of straight and bent amphibian and mammalian peripheral nerve *in vitro*: locus of excitation *J. Physiol.* **460** 201–19

[41] Woo S, Litzius K, Krüger B, Im M-Y, Caretta L, Richter K, Mann M, Krone A, Reeve R M and Weigand M 2016 Observation of room-temperature magnetic skyrmions and their current-driven dynamics in ultrathin metallic ferromagnets *Nat. Mater.* **15** 501

[42] Leonov A O, Monchesky T L, Romming N, Kubetzka A, Bogdanov A N and Wiesendanger R 2016 The properties of isolated chiral skyrmions in thin magnetic films *New J. Phys.* **18** 065003

[43] Tehovnik E J and Slocum W M 2009 Depth-dependent detection of microampere currents delivered to monkey V1 *Euro. J. Neurosci..* **29** 1477–89

[44] Zhou A, Santacruz S R, Johnson B C, Alexandrov G, Moin A, Burghardt F L, Rabaey J M, Carmena J M and Muller R 2019 A wireless and artefact-free 128-channel neuromodulation device for closed-loop stimulation and recording in non-human primates *Nat. Biomed. Eng.* **3** 15–26